JOURNAL OF
AGRICULTURAL AND
FOOD CHEMISTRY

Monitoring and Estimation of the Kinetics Parameters in the Binding Process of Tannic Acid to Bovine Serum Albumin with Electrochemical Quartz Crystal Impedance System

MEILING LIU, YOUYU ZHANG,* QIN YANG, QINGJI XIE,* AND SHOUZHUO YAO

Key Laboratory of Chemical Biology and Traditional Chinese Medicine Research (Ministry of Education), College of Chemistry and Chemical Engineering, Hunan Normal University, Changsha 410081, People's Republic of China

Combined measurements of piezoelectric quartz crystal impedance (PQCI) and electrochemical impedance (EI) were utilized in situ to monitor the adsorption of bovine serum albumin (BSA) onto the newly prepared Au colloid-modified electrode and study the binding process of tannic acid (TA) to BSA on the BSA-modified electrode surface. The time courses of the resonant frequency and the equivalent parameters of the sensor were simultaneously obtained during BSA adsorption and TA–BSA binding. Compared with the bare gold electrode, the Au colloid-modified gold electrode showed better biocompatibility, and the absorption capacity for BSA was increased by ~2.4 times. The observed frequency decrease was ascribed to the mass increase of the sensor surface resulting from the TA–BSA binding, which is believed to result mainly from the hydrogen bonding from FT-IR characterization. The maximal molar binding ratio of TA binding to immobilized BSA obtained from the frequency shift of the adsorbed BSA and TA was estimated to be 10.3:1. On the basis of the frequency decrease with time, the kinetics of the binding was quantitatively studied. By way of fitting the experimental data, the kinetics parameters, that is, binding and dissociation constant (k_1, k_{-1}), and the binding equilibrium constant (k_a) were determined, giving values of 9.51×10^4 M^{-1} s^{-1}, 3.15 s^{-1}, and 3.1×10^4 M^{-1}, respectively.

KEYWORDS: Tannic acid; bovine serum albumin; piezoelectric quartz crystal impedance; electrochemical impedance; electrochemical piezoelectric quartz crystal impedance system; FT-IR

INTRODUCTION

Polyphenols, especially tannins, are widely found in plant-derived feeds, beverages, foods, and medicines (*1*). The average dietary consumption of tannin is estimated to be over 50% of 1 g of the dietary polyphenols consumed daily by humans (*2*). However, the nutritional implications of tannins (plant polyphenols) for humans and animals are poorly understood (*3, 4*), and it is not yet known what properties of tannins affect the amino acid absorption (*5*). It is supposed that the propensity of tannin binding to proteins may affect tannin's bioavailability and/or mask the antioxidant capacity in vivo (*6*). Recently, tannin–protein interactions under both nonoxidizing and oxidizing conditions were reported to be vital to a balanced evaluation of the biological effect of tannin consumption (*7*). Under nonoxidizing conditions, tannin can form non-covalent complexes with proteins through hydrogen bonding or hydrophobic interactions (*8*), and a two-phase mechanism for the complex formation has been developed (*9*). The interactions of protein with tannin in this condition may reduce the digestibility of protein and contribute to reduce the oxygen species, which led to the suggestion of tannin as beneficial antioxidant consumption of

the plants by herbivore (*10*). While under oxidizing condition, tannin readily reacts with toxic reactants (*11*). Therefore, in this condition, the process of tannin reacting with protein to form a tannin–protein complex is disrupted by protein denaturants (*12*). From the existing literature, it is found that tannins are not universal protein-binding agents, and the binding affinity of tannins to proteins can vary (*13*); therefore, the structure–activity relationships appear to be important to protein–tannin interactions (*7, 14*).

Many techniques have been used to study the interaction between tannin and protein. X-ray crystallography (*15*), NMR spectroscopy (*6*), isothermal titration microcalorimetry (*17*), and nephelometry (*18*) were used to investigate the interaction between tannin and protein. Results from X-ray crystallography and NMR spectroscopy suggested that the protein–tannin interaction is initially driven by hydrophobic effects, and the complexes are stabilized by hydrogen bonding (*15, 16*). These techniques have been proved to be sensitive, selective, and feasible for a direct measure of insoluble aggregate in solution. However, they are not in situ techniques and cannot provide real-time information of the binding process.

With the advantages of high sensitivity, simplicity of use, and capability of providing multidimensional information for reflecting the physical and/or chemical properties of the

* Corresponding author (fax +86-731 8865515; telephone +86-731 8865515; e-mail zhangyy@hunnu.edu.cn).

investigated system, the piezoelectric quartz crystal impedance (PQCI) analysis technique has recently been widely used in life science, including protein adsorption (*19*), antibody immuno-assay (*20*), enzyme detection (*21*), DNA hybridization (*22, 23*), drug−DNA binding reaction (*24, 25*), DNA oxidative damage (*26*), bacteria detection (*27*), and so on. The PQCI analysis was based on the Butterworth−van Dyke (BVD) equivalent electrical circuit that contains the motional arm (the motional resistant R_1, the motional capacitance C_1, and the motional inductance L_1, in series), in parallel with the static arm (the static capacitance C_0). The four equivalent parameters have distinct physical meanings (*28−32*). Besides the four equivalent circuit parameters, the resonance frequency f_0 ($f_0 = 1/[2\pi(L_1C_1)^{1/2}]$) and the half-peak width of a $G−f$ curve ($\Delta f_{G1/2}$) (*33, 34*) were used to analyze the PQC response. The PQC sensor is sensitive to the change in mass on electrode, viscoelastic properties of film, and the density/viscosity of the test solution. For loading or removal of a rigid, thin, and homogeneous film on the PQC sensor, the frequency−mass relationship is described by the Sauerbrey equation (*35*)

$$-\Delta f_0 = 2.26 \times 10^{-6} f_{0g}{}^2 \frac{\Delta m}{A} \qquad (1)$$

where Δf_0 and f_{0g} are the frequency shift and the fundamental frequency of the quartz crystal in Hz, respectively; Δm is the mass loaded on the electrode in g, and A is the geometric area of the electrode in cm^2. The net density and viscosity effects on 9 MHz piezoelectric quartz crystal resonance were described by Martin equations (*29*). The relationship between the motional resistance change and the frequency shift can be expressed as

$$\Delta R_{1l} = -\frac{4\pi L_q \Delta f_{0l}\sqrt{f\mu_q}}{\sqrt{\bar{c}_{66}f_{0g}}} \approx -4\pi L_q \Delta f_{0l} \qquad (2)$$

where L_q and f_{0g} are the motional inductance and resonant frequency of the quartz crystal in air, respectively; μ_q is the shear modulus of the AT-cut quartz (2.947×10^{10} N/m^2); and $\bar{c}_{66}$ is the lossy piezoelectrically stiffened quartz elastic constant (2.957×10^{10} N/m^2). According to the above equation, the absolute value of the characteristic slope, $\Delta f_0/\Delta R_1$, for a net density/viscosity effect on the 9 MHz PQC resonance is $\sim$10 Hz Ω^{-1}.

Electrochemical impedance spectroscopy (EIS) measurement is a powerful electrochemical technique for the investigation of electrode processes through adopting smaller electrochemical perturbations, compared with some transient electrochemical techniques (*36*). This method allows the measurements of the electrolyte resistance (R_e) and the interfacial capacitance (C_s) of electrode/solution interface and, therefore, can be used to study the kinetics of protein adsorption onto the electrode surface (*37*) and monitor the binding process of small molecules to protein.

Thus, the combination of PQCI and electrochemical methods, namely, an electrochemical quartz crystal impedance system (EQCIS), which provides multidimensional piezoelectric information during electrochemical perturbations, has been used to study the adsorption of lysozyme onto bare Au electrode and the modified Au electrodes (*33*), cystine precipitation onto a Au electrode surface (*34*), metal and polymer deposition (*38*), and depletion-layer effects (*39*). In our previous research, the method combined with fluorescence spectrophotometry was used to reveal some basic aspects of the mechanism of TA interaction with proteins in solution (*40*). Because the response of TA interaction with the BSA modified electrode surface was small, we failed to study the kinetics of the process. Therefore,
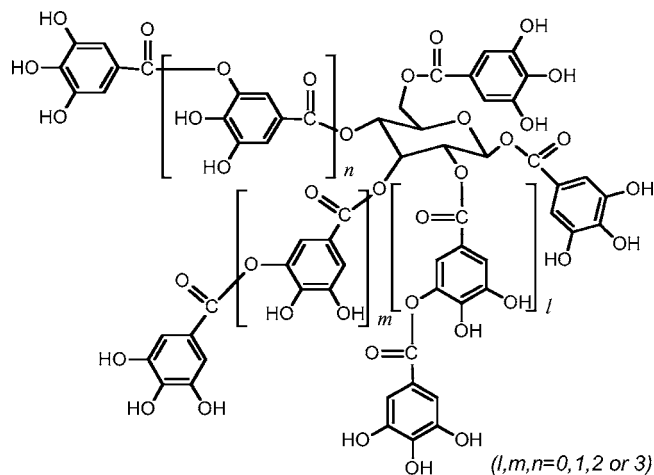

Figure 1. Chemical structure of TA.

in this work, we further investigated TA−BSA binding on the newly prepared BSA-immobilized gold nanoparticle surface. The time courses of the resonant frequency and the equivalent circuit parameters of the quartz crystal sensor during the binding process were simultaneously obtained and discussed. According to the decease of frequency with time, the kinetics of the binding was quantitatively studied by EQCIS, and the kinetics parameters, that is, the binding constant (k_1), the dissociation constant (k_{-1}), and the binding equilibrium constant (k_a), were also estimated.

MATERIALS AND METHODS

1,6-Hexanedithiol (97%) and BSA (molar weight, 67000) were purchased from Sigma and not purified before use. HAuCl$_4$·3H$_2$O (>99%) and tannic acid (molar weight, 1701.4) were purchased from Shanghai Reagent Co. The tannic acid (TA) is typical hydrolyzable tannin, a mixed gallotannin composed of gallic acid esters of glucose as shown in **Figure 1**. Sodium citrate, K$_4$Fe(CN)$_6$, absolute ethanol, and all other chemical reagents were of analytical grade or better quality. A 0.5% 1,6-hexanedithiol solution was prepared by dissolving it in absolute ethanol. NaAc−HAc buffer solution (pH 5.1) was obtained by mixing 0.1 M HAc and 0.2 M NaAc together. Stock solutions of BSA and TA were all prepared from the buffer solution and stored at 4 °C for further use. All other solutions were prepared with double-distilled water.

An HP4395A network/spectrum/impedance analyzer, a CHI 660A electrochemical workstation, and two IBM-compatible personal computers were used to constitute the EQCIS experimental setup. The conductance (G) and susceptance (B) data of the PQC resonance were recorded synchronously via an HP−IB interface card for Windows 3.1/NT/95 on the HP4395A. On the basis of the simultaneous fitting of both the G and B data to the BVD, the parameters of equivalent circuit and the resonant frequency were acquired by a user program written in Visual Basic (VB) 5.0. Electrochemical measurements were conducted on a conventional three-electrode cell comprising a gold PQC working electrode, a saturated calomel electrode (SCE) as reference electrode with a supporting electrolyte salt bridge, and a carbon rod counter electrode. AT-cut quartz crystal (9 MHz, 12.5 mm in diameter) with gold electrodes (6 mm in diameter) on both sides was used, one side immersed in the test solution as the working electrode and the other side placed in the air. The TU-1221 UV−vis spectra recording spectrophotometer was used to measure the absorbency spectra of Au colloid. The IR spectra were collected on a pressed pellet with KBr in the transmission mode on a Nicolet Nexus 670 FTIR spectrometer (Nicolet Instrument Co., Madison, WI) controlled by Ominic software. All experiments were carried out at room temperature.

Preparation of Au Nanparticles. All glassware was cleaned with freshly prepared HNO$_3$ + HCl (v/v 3:1), rinsed thoroughly with double-distilled water, and dried in the air. Au colloid particles were prepared according to the literature (*41*) and then stored in the dark at 4 °C for further use.
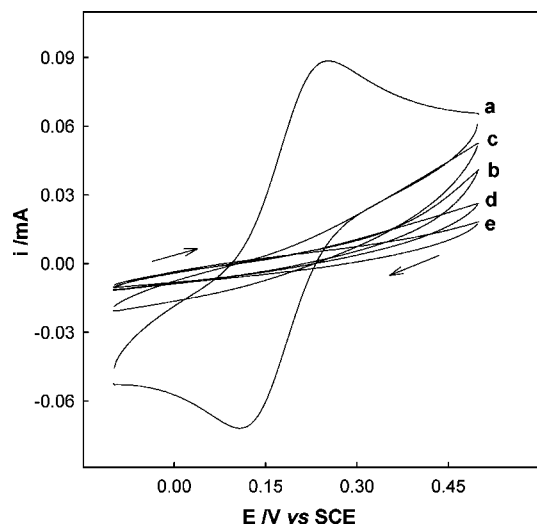
Binding Process of Tannic Acid to BSA

J. Agric. Food Chem., Vol. 54, No. 12, 2006 **4089**

Figure 2. Cyclic voltammograms for bare (**a**) and Au/SAM- (**b**), Au/SAM/NG- (**c**), Au/SAM/NG/BSA- (**d**), and Au/SAM/NG/BSA/TA-modified (**e**) Au electrode in 0.1 M Na_2SO_4 solution containing 2.0 mM $K_4Fe(CN)_6$ at a scan rate of 50 mV s^{-1}. Arrows indicate the scan direction.

Figure 3. Electrochemical impedance spectrum for bare (**a**), Au/SAM- (**b**), Au/SAM/NG- (**c**), Au/SAM/NG/BSA- (**d**), and Au/SAM/NG/BSA/TA-modified (**e**) Au electrode in 0.1 M Na_2SO_4 solution containing 2.0 mM $K_4Fe(CN)_6$. Conditions: 100 kHz–0.1 Hz, 5 mV rms, 0.1 V vs SCE.

Preparations of the 1,6-Hexanedithiol Self-Assembled Monolayer (SAM) and the Au Nanoparticle-Modified Electrode. To remove possible contamination, the surfaces of the gold electrodes were treated with piranha solution (98% H_2SO_4 + 30% H_2O_2) for 5 min. After the treatment, the sensor was rinsed thoroughly with double-distilled water and ethanol and dried under nitrogen. A 0.5% 1,6-hexanedithiol solution (5 μL) was dropped onto the surface of the PQC sensor and dried in the dark. Then 15 μL of Au colloid solution was dropped onto the 1,6-hexanedithiol-modified electrode surface for ~6 h until it dried, and the Au/SAM/NG electrodes were obtained.

Immobilization of BSA onto the Au/SAM/NG Electrode. The Au/SAM/NG electrode was placed in the NaAc−HAc buffer solution (pH 5.1) for a given time until its piezoelectric response parameters, such as f_0, R_1, and C_0, became stable. BSA stock solution (0.15 mL of 0.1 g/mL) was added to the solution under magnetic stirring, which led to a final BSA concentration of 0.4 mg/mL. The adsorption process was monitored by the EQCIS until the resonant frequency of the PQC electrode in solution became stable.

Monitoring the Binding of TA to BSA. The BSA/Au/SAM/NG-modified electrode was placed in NaAc−HAc buffer solution (pH 5.1). After the piezoelectric response parameters of the sensor became stable, a given volume of stock solution of TA was added into the buffer solution. The corresponding final concentrations of TA in the detection cell were 5, 15, 25, 35, and 45 μM, respectively. The response parameters during the interaction between TA and BSA were recorded by EQCIS. For studying the effect of the concentration of TA on the binding, a given volume of stock solution of TA was added every 200 s.

RESULTS AND DISCUSSION

Characterization of the Gold Nanoparticles and the SAM-Modified Electrode. The freshly prepared gold nanoparticles were characterized by UV−vis spectrum, and the maximum absorbance peak appeared at 516 nm. This result suggested that the $HAuCl_4$ was reduced to nanogold (*41*).

It is well-known that SAM can be adsorbed on the Au surface by a thiol group (*42*). In our experiment, the frequency shift decreased by ~150 Hz after 1,6-hexanedithiol was adsorbed on the gold electrode surface, whereas after the immobilization of Au colloids, the frequency of the sensor in the air decreased by ~1500 Hz. To check the quality of the SAM and the Au colloid layer, cyclic voltammetric study and the electrochemical impedance experiments were preformed. **Figure 2** shows the cyclic voltammogram of the bare gold electrode, the SAM-modified electrode, and the Au/SAM/NG electrode in 2 mM
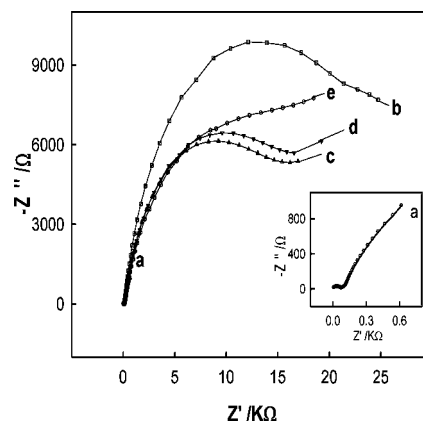
$K_4Fe(CN)_6$ (0.1 M Na_2SO_4 as electrolyte) solution, respectively. It can be seen that the peaks of the reduction of $[Fe(CN)_6]^{3-}$ and the oxidation of $[Fe(CN)_6]^{4-}$ disappeared after the 1,6-hexanedithiol covered the gold electrode surface. A nearly unobservable faradic current suggested that the film of 1,6-hexanedithiol was densely packed and almost defect-free. Such a SAM layer essentially blocked the electronic communication between the $[Fe(CN)_6]^{4-}$ in the solution and the underlying Au electrode. This result was consistent with previous reports of Wang et al. (*42*). As can be seen from the plot, the enhancement of the electronic transfer rate of $[Fe(CN)_6]^{4-}$ was not obvious after the adsorption of Au colloid on the SAM. Thus, it was apparent that when a densely packed alkanethithiol or alkanedithiol SAM was formed, the electronic transfer would be greatly blocked (*43*). When the electrode was modified with alkanethiol-capped Au nanoparticles, defects might exist within the particle array (*42*). In addition, **Figure 3** shows the electrochemical impedance spectroscopy before and after the layer-by-layer assembled. The typical shape of Nyquist impedance spectra includes a semicircle followed by a straight line. In general, two frequency regions can be distinguished in the presence of the electroactive species. The semicircular portion observed at the higher frequencies corresponds to an electron-transfer-limited process, whereas the straight line represents the diffusion-limited process. In this experiment, a large increase in the diameter of the semicircle of the electrochemical impedance spectrum (**Figure 3b**) was observed after adsorption of 1,6-hexanedithiol on the Au electrode surface, compared with the bare Au electrode (**Figure 3a**). This result suggested that the reversibility of the $[Fe(CN)_6]^{3-}/[Fe(CN)_6]^{4-}$ decreased, the gold surface was packed by 1,6-hexanedithiol molecules, and the electron-transfer ability weakened. After the gold nanoparticles immobilized on the 1,6-hexanedithiol-modified surface, the diameter of the semicircle was decreased (**Figure 3c**). These results agreed well with the cyclic voltammogram in **Figure 2**.

Investigation of BSA Immobilization. Our previous fluorescence experiment showed that BSA was stable in the solution with pH value from 4 to 8 (*40*), so pH 5.1 was chosen in our experiment. The typical response of the parameters of the Au/SAM/NG modified PQC in the BSA adsorption process is shown in **Figure 4**. The addition of BSA into the tested solution resulted in significant change in all parameters. The frequency decreased quickly and the resistance increased. After ~20 min, all of the parameters of the PQC became stable, which meant that the adsorption had reached equilibrium. According to **Figure 4**, the $\Delta f_0/\Delta R_1$ ratio for BSA adsorption on Au/SAM/
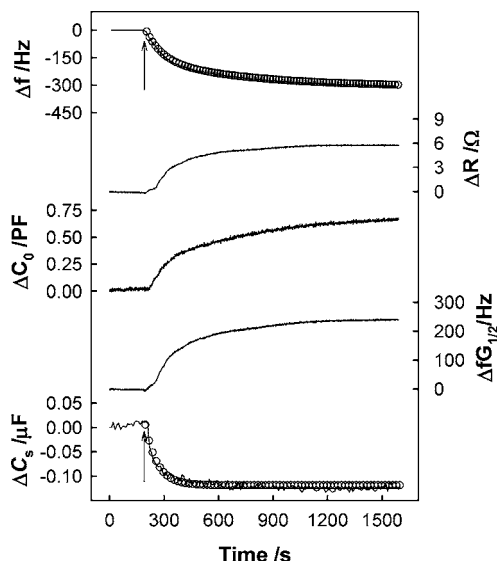
Figure 4. Typical time courses of simultaneous response of the parameters of the PQC sensor during BSA adsorption onto the Au/SAM/NG electrode in 0.1 M HAc + 0.2 M NaAc buffer solution (pH 5.1). The final concentration of BSA was 0.4 g/L. The electrochemical impedance conditions were 3 kHz, 5 mV rms, and 0 V versus SCE. Arrows indicate the addition of BSA in the detection cell.

NG electrodes was estimated to be ~-54 Hz Ω^{-1}. This indicated that the mass change took a dominant effect on the total frequency shift, and the Sauerbrey equation was reasonably valid under our experimental conditions. Thus, the frequency shift can be used to calculate the approximate amount of the adsorbed proteins. The adsorption behavior of BSA on the Au/SAM/NG electrode was similar to that of BSA adsorption on the bare gold electrode (*40*), which contained two consecutive reactions at the interface. However, the frequency shift during BSA adsorption on the Au/SAM/NG electrode was ~2.4 times that of the bare Au electrode (*40*). Because the colloid gold particle modified surface has a very high surface-to-volume ratio, the rougher surface can adsorb more BSA molecules. The surface of uncontaminated gold nanoparticles is very active and can give the protein molecules more freedom in the orientation and increase the possibility to make the prosthetic group closer to the metal particle surface (*44*). In addition, C_s could represent the interfacial capacitance according to a simplified R_s-C_s equivalent circuit in the absence of electrical active species (*36*). The ΔC_s of the electrode calculated through the imaginary part of the impedance of the electrochemical experiment decreased quickly with the process of BSA adsorbed onto the gold colloid surface. This might result from the adsorption occurring on the surface, which changed its hydrophilic/hydrophobic surface properties. The response (*r*) can be expressed as a sum of two exponential functions:

$$r(t) = a_0 + a_1\, e^{-t/t_1} + a_2\, e^{-t/t_2} \qquad (3)$$

Taking a_0, a_1, a_2, t_1, and t_2 as estimation parameters, we fitted Δf_0 and ΔC_s with a Sigmaplot V2.0 nonlinear fitting program. The best fitted parameters were -316, 151, 164, 536, and 88 for Δf_0 and -0.123, -5.69, 5.81, 74.4, and 74.4 for ΔC_s, respectively. The fitted curves were consistent with the experimental result, as circles shown in **Figure 4**.

Typical Response Curves of TA Binding to BSA. Figure 5 shows the typical response of piezoelectric quartz crystal resonance during TA binding to BSA immobilized on the Au/SAM/NG/BSA-modified PQC electrode. The addition of TA
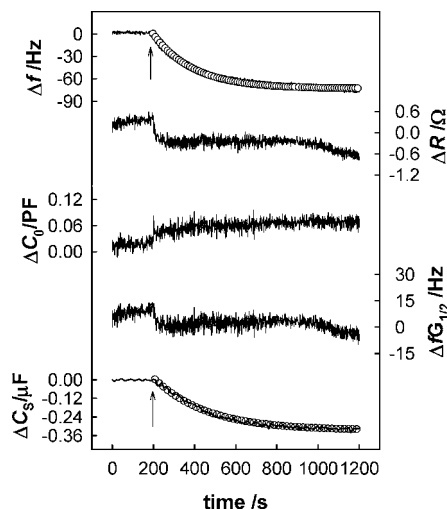

Figure 5. Response of the parameters of the PQC sensor with time during TA binding to BSA onto the BSA-modified electrode surface in 0.1 M HAc + 0.2 M NaAc buffer solution (pH 5.1). The electrochemical impedance conditions were 3 kHz, 5 mV rms, and 0 V versus SCE. Arrows indicate the addition of BSA in the detection cell.

led to a large decrease in f_0 and C_0 and a small decrease in R_1. C_0 increased due to the change of the capacity and/or structure of the electrical double layer at the interface. The change of R_1 and $\delta f_{G1/2}$ reflected the viscosity change of the solution or the film deposited on the electrode. The f_0 during the binding of TB to BSA was decreased by ~83 Hz. The absolute value of $\Delta f_0/\Delta R_1$ was 102 Hz Ω^{-1}, which is >10 Hz Ω^{-1}, suggesting that the mass effect dominated the frequency change. Therefore, the change in the viscosity of the adsorbed film and the density or viscosity of the solution induced by the addition of TA contributing to the changes in R_1 and $\delta f_{G1/2}$ could be neglected. Hence, the observed decrease in f_0 should be mainly ascribed to the mass increase of the surface. In addition, there was no frequency decrease when NaAc−HAc solution was added into the detection cell in our experiment. Thus, the frequency shift should be ascribed to the interaction of TA to BSA, and the mass of TA could be calculated according to the Sauerbery equation. The Δf_0-t curve corresponding to the binding process represents the kinetics of the binding. In addition, the electrochemical impedance experiments showed that the interfacial capacitance (ΔC_s) decreased quickly when TA was added into the detection solution. This might result from the formation of TA−BSA complex, which led fewer water molecules to penetrate into the electrical double layer and thus resulted in an observable decrease of C_s. To our knowledge, TA is a weak acid (pK_a 9−10), indicating practically there were positive charges at pH 5.1. Although the isoelectric point of BSA is 4.8, its net charge was near zero in our experimental conditions. Therefore, the interaction between TA and BSA might not be due to the electrostatic interaction. Oh et al. suggested their interaction was hydrophobic or hydrogen bond cross-linking (*15*). To determine the main interaction between BSA and TA, we collected the IR spectra of BSA, TA, and TA−BSA complex, as shown in **Figure 6**. In IR spectra of the TA−BSA complex, the peaks at 1317, 1198, 1071, and 761 cm^{-1} in the spectra of the complex are the characters of TA, which suggested that the interaction between BSA and TA had occurred. Compared with the pure IR spectra of BSA, the stretch vibration of N−H shifted from 3382 to 3332 cm^{-1}, and amide I (1655 cm^{-1}) and amide II (1542 cm^{-1}) also red shifted. Because amide II was more sensitive, it shifted by ~12 cm^{-1}. All of these results indicated that the hydrogen bond was formed between BSA and TA. Therefore, we supposed that the hydrogen bonding
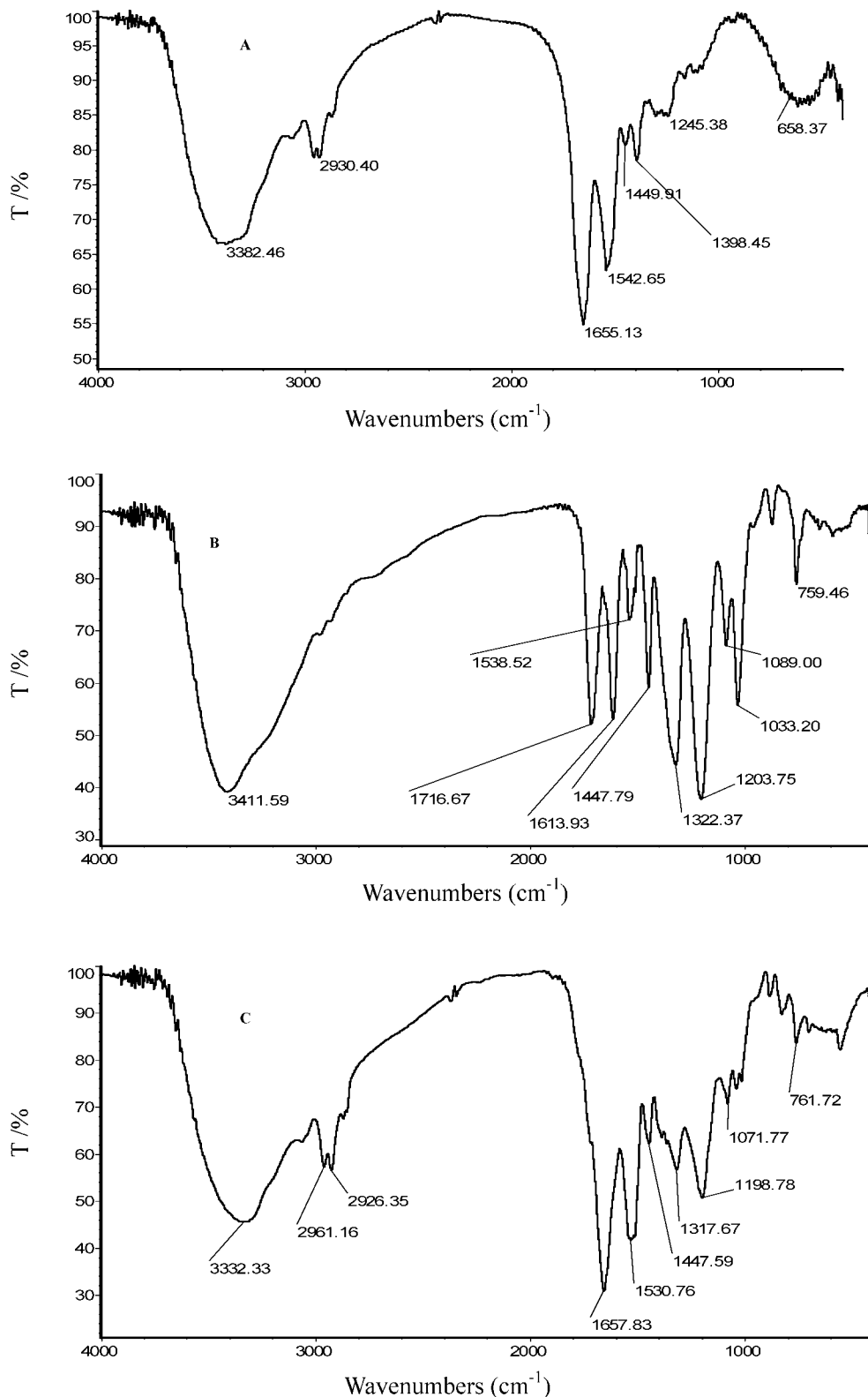
Binding Process of Tannic Acid to BSA

J. Agric. Food Chem., Vol. 54, No. 12, 2006 **4091**

Figure 6. IR spectra of (**A**) BSA, (**B**) TA, and (**C**) BSA–TA complex.

was the major interaction of TA−BSA binding, and the nature of the interaction may be that the several phenolic hydroxyl groups in TA interacted with BSA through the formation of strong hydrogen bond cross-linking.

The cyclic voltammogram and the electrochemical impedance spectra (shown in **Figures 2d,e** and **3d,e**) were conducted in $Fe(CN)_6^{4-}$ solution after the immobilization of BSA and TA−BSA binding. It was clear that the redox couple of the Fe-

$(CN)_6^{3-}/Fe(CN)_6^{4-}$ exhibited a more irreversible behavior after TA−BSA binding, suggesting that the electrode surface was occupied by the TA−BSA complex to a significant extent and the electron exchange ability on the electrode became weaker. Therefore, the results showed that the interface properties of the film changed after BSA immobilization on the Au/SAM/ NG electrode and the TA−BSA binding. They also suggested that the interaction between TA and BSA occurred.
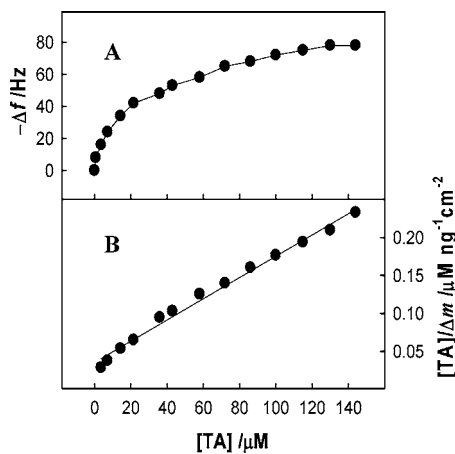
Figure 7. Relationships of saturation binding of TA to the Au/SAM/NG/BSA electrode surface to concentration (**A**) and $[TA]_0/\Delta m$ to $[TA]_0$ (**B**).

Kinetic Study of TA−BSA Binding Process. When the concentration of TA was increased in the solution, the relationship between the binding amount of TA (Δm) corresponding to the change of frequency and its concentration in the solution showed a simple saturation curve (as shown in **Figure 7A**). The relationship of $[TA]_0/\Delta m$ to $[TA]_0$ described in eq 4 is shown in **Figure 7B**.

$$\frac{[TA]_0}{\Delta m} = \frac{[TA]_0}{\Delta m_{max}} + \frac{1}{\Delta m_{max} k_a} \tag{4}$$

$[TA]_0$ indicates the initial concentration of TA. From eq 4, the relationship of $[TA]_0/\Delta m$ to $[TA]_0$ is linear. According to our experiment, a linear relationship of $[TA]_0/\Delta m$ and $[TA]_0$ was also obtained. The association constants (k_a) and the maximum binding amount (Δf_{max}) of TA to BSA were calculated from the slope and the intercept of the line. Therefore, the values of k_a and Δf_{max} are 3.2×10^4 and -83 Hz, respectively. The binding molar ratio can be calculated according to the following equation:

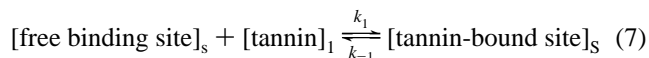$$\frac{n_{tannin}}{n_{BSA}} = \left(\frac{W_{tannin}}{M_{tannin}}\right) : \left(\frac{W_{BSA}}{M_{BSA}}\right) \tag{5}$$

By combination of the frequency response and the Sauerbrey equation (*29*), the following equation can be obtained:

$$n_{tannin} : n_{BSA} = \frac{M_{BSA} \times \Delta f_{0,tannin}}{M_{tannin} \times \Delta f_{0,BSA}} \tag{6}$$

In eq 6 n_{TA} and n_{BSA} are the amounts of TA and BSA in mol, W_{TA} and W_{BSA} are the masses of TA and BSA on the electrode surface in g, M_{TA} and M_{BSA} are molar masses of TA and BSA, which are 1701.4 and 67000, respectively, and $\Delta f_{0,BSA}$ (-316 Hz in this case) and $\Delta f_{0,TA}$ (-83 Hz in this case) are the frequency shifts caused by the adsorption of BSA and the TA interaction with BSA, respectively. The molar ratio of TA to the immobilized BSA calculated through eq 6 was about 10.3:1.

The kinetics constants of TA binding to BSA can also be calculated from the relationship of frequency decrease to time (mass increase) shown in **Figure 5**. In general, the drug−protein binding is reversible and rapid (*45*). From the Δf_0-t curves in **Figure 5**, we supposed that the binding between TA and immobilized BSA on the Au/SAM/NG electrode surface could be described by the following equation similar to the equation used by Mao et al. (*25*):

$$[\text{free binding site}]_s + [\text{tannin}]_l \underset{k_{-1}}{\overset{k_1}{\rightleftharpoons}} [\text{tannin-bound site}]_S \tag{7}$$

Here $[\text{tannin}]_l$ and $[\text{free binding site}]_s$ are species in the solution and on the surface of the sensor, respectively. k_1 and k_{-1} are the binding and dissociation rate constants of the binding species (e.g., tannin-bound site in BSA), respectively. Before injection of the TA sample, there were a certain number of BSA sites on the electrode surface, and the sites attacked by TA were constant, but with the progression of interaction between TA and BSA at the liquid/solid interface, the number of active sites of BSA continued to decrease. The interaction rate was assumed to be proportional to the active surface area that was attacked by TA. The binding amount formed at time t after the addition of TA is given by

$$\theta_t = \theta_e(1 - e^{-(1/\tau)t}) \tag{8}$$

The equilibrium percentage θ_e corresponds to the maximum percentage of the TA-bound active sites. Moreover, the increase in θ_t results in a mass increase of the sensor surface. Therefore, the following equation can be obtained

$$\Delta m_t = \Delta m_{max}(1 - e^{-(1/\tau)t}) \tag{9}$$

In eq 9 Δm_t and Δm_{max} are the mass increases of the sensor surface at time t and $t \rightarrow \infty$ (or at the time of binding equilibrium), respectively. According to the previous discussion, the frequency decrease is mainly ascribed to the mass increase. Therefore, eq 9 can be rewritten as

$$\Delta f_0 = \Delta f_{0,max}(1 - e^{-(1/\tau)t}) \tag{10}$$

where Δf_0 and $\Delta f_{0,max}$ are the frequency changes at time t and $t \rightarrow \infty$, respectively. This equation can be considered as the piezoelectric response model during the binding. Okahata et al. used an equation similar to eq 10 to study DNA hybridization (*23*) and investigate the specific binding of basic leucine-zipper (bZIP) motif of the yeast transcription factor GCN_4 to a duplex DNA (*46*). On the basis of eq 10, $\Delta f_{0,max}$ and the reciprocal of the relaxation time (τ^{-1}) in **Figure 5** can be obtained through fitting experiment data, and the fitting result is also shown as circles in **Figure 5**. The quality of the fitting can be evaluated with the relative sum of the residual square, q_r, defined as

$$q_r = \frac{\sum_1^N (\Delta f_{0,fit} - \Delta f_{0,expt})^2}{\sum_1^N \Delta f_{0,expt}^2} \tag{11}$$

where $\Delta f_{0,fit}$ and $\Delta f_{0,expt}$ refer to the values of frequency shift obtained by way of fitting method and experiment, respectively, and N is the number of the response signal points.

In addition, the following equation displays a relationship between the relaxation rate constant (τ^{-1}) and the initial TA concentration $[TA]_0$:

$$\tau^{-1} = k_1[TA]_0 + k_{-1} \tag{12}$$

If the binding processes at different TA concentrations were monitored, a series of τ^{-1} and $\Delta f_{0,max}$ can be obtained according to eq 10. Then, the kinetics parameters, k_1 and k_{-1}, can be
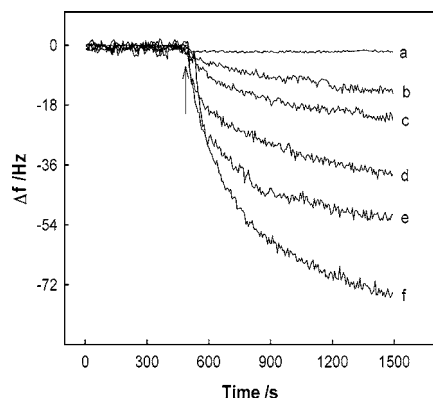
Binding Process of Tannic Acid to BSA

J. Agric. Food Chem., Vol. 54, No. 12, 2006 **4093**

Figure 8. Real-time frequency response curves for the binding processes of TA and BSA at different TA concentrations: (**a**) 0, (**b**) 5, (**c**) 15, (**d**) 25, (**e**) 35, and (**f**) 45 μmol L^{-1}. The arrow indicates time of TA addition.
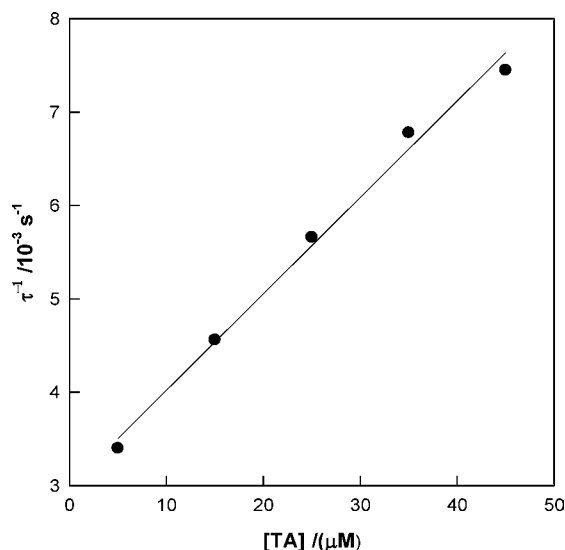

Figure 9. Linear reciprocal plot of rate constant τ^{-1} against the concentration of TA.

Table 1. Results Obtained by Fitting the Response Data in **Figure 7** to Equation 12

[TA]$_0$/μmolL^{-1}	$f_{0,max}$/Hz	τ^{-1} (10^{-3})	q_r
5	−13.5	3.30	1.20 × 10^{-3}
15	−20.5	3.78	8.20 × 10^{-3}
25	−36.0	4.62	1.08 × 10^{-3}
35	−50.0	5.66	4.78 × 10^{-3}
45	−73.0	6.21	1.99 × 10^{-3}

determined from eq 12, and the binding equilibrium constant, K_a, can be thus obtained:

$$k_a = k_1/k_{-1} \qquad (13)$$

Figure 8 shows the real-time frequency response curves for the TA−BSA binding process at different TA concentrations. By fitting these response data to eq 10, the values of $\Delta f_{0,max}$ and τ^{-1} were obtained (shown in **Table 1**). The small values of q_r indicated that the fitting results were in reasonable agreement with the corresponding experimental results. **Figure 9** shows a linear correlation between the reciprocal of the relaxation time (τ^{-1}) of the binding and the concentration of TA with a correlation coefficient of 0.997. The values of k_1 and k_{-1} were estimated from the slope and intercept to be 9.5 × 10^4 M^{-1} s^{-1} and 3.1 s^{-1}, respectively. The binding equilibrium constant K_a

was calculated to be 3.1 × 10^4 M^{-1}. The K_a value obtained from the curve-fitting method according to eq 13 was consistent with that obtained from the saturation method.

Conclusions. EQCIS was used in our experiment to monitor the immobilization of BSA on the newly prepared Au/SAM/NG electrode surface and the binding process of TA to BSA. The gold colloids exhibit good bioactivity and can adsorb more BSA molecules in our experimental condition. The binding process between BSA and TA was kinetic and rapid, and the interaction was mainly hydrogen bonding. The kinetics parameters during the TA−BSA binding, such as the binding constant (k_1), dissociation rate constant (k_{-1}), and binding amount could be obtained from the time dependencies of the frequency decrease. The binding mole ratio and the association constant ($k_a = k_1/k_{-1}$) were estimated to be 10.3:1 and (3.1 ± 0.1) × 10^4 M^{-1}, respectively. It was also found that EQCIS is a useful method to investigate the binding process of other small molecules or environmental toxicants to biomacromolecules. In addition, the relationship between the logarithmic value of the frequency shift and the concentration of TA based on **Figure 8** was found to be linear, and the equation is log Δf = 0.0185-[TA] + 1.05 (r = 0.9962; concentration of TA in μM), demonstrating that a PQC sensor for sensitive detection of TA may be constructed on the basis of the TA−BSA interaction; such research is in progress in this laboratory.

ABBREVIATIONS USED

BSA, bovine serum albumin; TA, tannic acid; PQCI, piezoelectric quartz crystal impedance; EI, electrochemical impedance; EIS, electrochemical impedance spectroscopy; EQCIS, electrochemical quartz crystal impedance system; IR, infrared; SAM, self-assembled monolayer; NG, gold nanoparticle.

LITERATURE CITED

(1) Haslam, E. *Practical Polyphenolics: From Stucture to Molecular Recognition and Physiological Action*; Cambridge University Press: Cambridge, U.K., 1998.

(2) Gonthier, M. P.; Donovan, J. L.; Texier, O.; Felgines, C.; Remesy, C.; Scalbert, S. Metabolism of dietary procyanidins in rats. *Free Radical Biol. Med.* **2003**, *35*, 837−844.

(3) Mueller-Harvey, I.; Mcallan, A. B. Tannins−their biochemistry and nutritional properties. In *Advances in Plant Cell Biochemistry and Biotechnology*; Morrison, I. M., Ed.; JAI Press: London, U.K., 1992; Vol. 1, pp 151−217.

(4) Duthie, G. G.; Duthie, S. J.; Kyle, J. A. M. Plant polyphenols in cancer and heart disease: implications as nutritional anti oxidants. *Nutr. Res. Rev.* **2000**, *13*, 79−106.

(5) Caygill, J. C.; Mueller-Harvey, I. *Secondary Plant Products− Antinutritional and Beneficial Actions in Animal Feeding*; Nottingham University Press: Nottingham, U.K., 1999; p 129.

(6) Sirafini, M.; Ghiselli, A.; Ferro-Luzzi, A. In vivo antioxidant effect of green and black tea in man. *Eur. J. Clin. Nutr.* **1996**, *50*, 28−32.

(7) Chen, Y.; Hagerman, A. E. Quantitative examination of oxidized polyphenol−protein complexes. *J. Agric. Food Chem.* **2004**, *52*, 6061−6067.

(8) Hagerman, A. E.; Rice, M. E.; Ritchard, N. T. Mechanisms of protein precipitation for two tannins, pentagalloyl glucose and epicatechin$_{16}$ (4−8) catechin (procyanidin). *J. Agric. Food Chem.* **1998**, *46*, 2590−2595.

(9) Bi, J. L.; Felton, G. W.; Murphy, J. B.; Howles, P. A.; Dixon, R. A.; Lamb, C. J. Do plant phenolics confer resistance to specialist and generalist insect herbivores? *J. Agric. Food Chem.* **1997**, *45*, 4500−4504.

(10) Charlton, A. J.; Baxter, N. J.; Khan, M. L.; Moir, A. J. G.; Haslam, E.; Davies, A. P.; Williamson, M. P. Polyphenol/peptide binding and precipitation. *J. Agric. Food Chem.* **2002**, *50*, 1593−1601.

4094 *J. Agric. Food Chem.,* Vol. 54, No. 12, 2006

Liu et al.

(11) Bors, W.; Foo, L. Y.; Hertkorn, N.; Michel, C.; Stettmaier, K. Chemical studies of proanthocyanidins and hydrolyzable tannins. *Antioxid. Redox Signaling* **2001**, *3*, 995−1008.

(12) Stern, J. L.; Hagerman, A. E.; Steinberg, P. D.; Mason, P. K. Phlorotannin−protein interactions. *J. Chem. Ecol.* **1996**, *22*, 1877−1899.

(13) Hagerman, A. E.; Butler, L. G. The specificity of proanthocyanidin−protein interaction. *J. Biol. Chem.* **1981**, *256*, 4494−4497.

(14) de Freitas, V.; Mateus, N. Structural features of procyanidin interactions with salivary proteins. *J. Agric. Food Chem.* **2001**, *49*, 940−945.

(15) Oh, H. I.; Hoff, J. E.; Armstrong, G. S.; Haff, L. A. Hydrophobic interaction in tannin−protein complexes. *J. Agric. Food Chem.* **1980**, *28*, 394−398.

(16) Haslam, E. Natural polyphenols (vergitable tannins) as drugs: possible modes of action. *J. Nat. Prod.* **1996**, *59*, 205−215.

(17) Frazier, R. A.; Papadopoulou, A.; Mueller-Harvey, I.; Kissoon, D.; Green, R. J. Probing protein−tannin interactions by isothermal titration microcalorimetry. *J. Agric. Food Chem.* **2003**, *51*, 5189−5195.

(18) Mateus, N.; Carvalho, E.; Luis, C.; de Freitas, V. Influence of the tannin structure on the disruption effect of carbohydrates on protein−tannin aggregates. *Anal. Chim. Acta* **2004**, *513*, 135−140.

(19) Yang, M.; Chung, F. L.; Thompson, M. Acoustic network analysis as a novel technique for studying protein adsorption and denaturation at surfaces. *Anal. Chem.* **1993**, *65*, 3713−3716.

(20) Fung, Y. S.; Wong, Y. Y. Self-assembled monolayers as the coating in a quartz piezoelectric crystal immunosensor to detect salmonella in aqueous solution. *Anal. Chem.* **2001**, *73*, 5302−5308.

(21) Bao, L.; Xie, Q.; Wu, Y.; Wei, W. A method for determination of α-amylase with a bulk acoustic wave sensor. *Anal. Lett.* **1999**, *32*, 885−889.

(22) Caruso, F.; Rodda, E.; Furlong, D. N.; Niikura, K.; Okahata, Y. Quartz crystal microbalance study of DNA immobilization and hybridization for nucleic acid sensor development. *Anal. Chem.* **1997**, *69*, 2043−2049.

(23) Okahata, Y.; Kawase, M.; Niikura, K.; Ohtake, F.; Furusawa, H.; Ebara, Y. Kinetic measurements of DNA hybridization on an oligonucleotide-immobilized 27-MHz quartz crystal microbalance. *Anal. Chem.* **1998**, *70*, 1288−1296.

(24) Su, H.; Williams P.; Tompson, M. Platinum anticancer drug binding to DNA detected by thickness-shear-mode acoustic wave sensor. *Anal. Chem.* **1995**, *67*, 1010−1013.

(25) Mao, Y.; Wei, W.; He, D.; Nie, L.; Yao, S. Monitoring and kinetic parameter estimation for the binding process of berberine hydrochloride to bovine serum albumin with piezoelectric quartz crystal impedance analysis. *Anal. Biochem.* **2002**, *306*, 23−30.

(26) Guo, B.; Yuan, Y.; Wu, Y.; Xie, Q.; Yao, S. Assay and analysis for anti- and pro-oxidative effects of ascorbic acid on DNA with the bulk acoustic wave impedance technique. *Anal. Biochem.* **2002**, *305*, 139−148.

(27) Wu, Y.; Xie, Q.; Zhou, A.; Zhang, Y.; Nie, L.; Yao, S., Mo, X. Detection and analysis of *Bacillus subtilis* growth with piezoelectric quartz crystal impedance based on starch hydrolysis. *Anal. Biochem.* **2000**, *285*, 50−57.

(28) Muramatsu, H.; Tamiya, E.; Karube, I. Computation of equivalent circuit parameters of quartz crystals in contact with liquids and study of liquid properties. *Anal. Chem.* **1988**, *60*, 2142−2146.

(29) Martin, S. J.; Granstaff, V. E.; Frye, G. C. Characterization of a quartz crystal microbalance with simultaneous mass and liquid loading. *Anal. Chem.* **1991**, *63*, 2272−2281.

(30) Thompson, M.; Kipling, A. L.; Duncan-Hewitt, W. C.; Rajakovic, L. V.; Cabic-Vlasak, B. A. Thickness-shear-mode acoustic wave sensors in the liquid phase. *Analyst* **1991**, *116*, 881−890.

(31) Bandey, H. L.; Gonsalves, M.; Hillman, A. R.; Glidle, A.; Bruckenstein, S. Dynamic quartz crystal impedance measurements of polyvinylferrocene film deposition. *J. Electroanal. Chem.* **1996**, *410*, 219−227.

(32) Buttry, D. A. In *Electroanalytical Chemistry*; Bard, A. J., Ed.; Dekker: New York, 1999; Vol. 17.

(33) Zhang, Y.; Xie, Q.; Zhou, A.; Yao, S. In situ monitoring of losozyme adsorption onto bare and cysteine- or 1-octadecanethiol-modified Au electrodes using an electrochemical quartz-crystal impedance system. *Anal. Sci.* **2000**, *16*, 799−805.

(34) Xie, Q.; Zhang, Y.; Yuan, Y.; Guo, Y.; Wang, X.; Yao, S. An electrochemical quartz crystal impedance study on cysteine precipitation onto an Au electrode surface during cysteine oxidation in aqueous solution. *J. Electroanal. Chem.* **2000**, *484*, 41−54.

(35) Sauberbuey, G. Verwendung von Schwingquarzen zur Wägung dünner Schichten und zur Mikrowägung. *Z. Phys.* **1959**, *155*, 206−222.

(36) Bard, A. J.; Faulkner, L. R. *Electrochemical Methods: Fundamentals and Applications*; Wiley: New York, 1980.

(37) Bernabeu, P.; Tamisier, L.; Cesare, A. De.; Caprani, A. Study of the adsorption of albumin on a platinum rotating disk electrode using impedance measurements. *Electrochim. Acta* **1988**, *33*, 1129−1136.

(38) Xie, Q.; Xiang, C.; Zhang, Y.; Yuan, Y.; Liu, M.; Nie, L.; Yao, S. In situ monitoring of goldsurface adsorption and acidic denaturation of human serum albumin by an isolation capacitance-adopted electrochemical quartz crystal impedance system. *Anal. Chim. Acta* **2002**, *464*, 65−77.

(39) Xie, Q.; Wang, J.; Zhou, A.; Zhang, Y.; Liu, H.; Xu, Z.; Yuan, Y.; Deng, M.; Yao, S. A study of depletion layer effects on equivalent circuit parameters using an electrochemical quartz crystal impedance system. *Anal. Chem.* **1999**, *71*, 4649−4656.

(40) Zhang, Y.; Wang, M.; Xie, Q.; Wen, X.; Yao, S. Monitoring of the interaction of tannin with bovine serum albumin by electrochemical quartz-crystal impedance system and fluorescence spectrophotometry. *Sens. Actutors B* **2005**, *105*, 454−463.

(41) Doron, A.; Katz, E.; Willner, I. Organization of Au colloids as monolayer films onto ITO glass surfaces: application of the metal colloid films as base interfaces to construct redox-active monolayers. *Langmuir* **1995**, *11*, 1313−1317.

(42) Wang, J.; Wu, H.; Angnes, L. On-line monitoring of hydrophobic compounds at self-assembled monolayer modified amperometric flow detectors. *Anal. Chem.* **1993**, *65*, 1893−1896.

(43) Yang, M.; Zhang, Z. Impediment to heterogeneous electron-transfer reactions of redox-active species by alkanedithiol self-assembled monolayers with and without an adlayer of Au nanoparticles. *Electrochim. Acta* **2004**, *49*, 5089−5095.

(44) Long, Y.; Nie, L.; Chen, J.; Yao, S. Piezoelectric quartz crystal impedance and electrochemical impedance study of HAS-diazepam interaction by nanogold-structured sensor. *J. Colloid Interface Sci.* **2003**, *263*, 106−112.

(45) Huang, Y.; Zhang, Z.; Zhang, D.; Lv, J. Flow-injection analysis chemiluminescence detection combined with microdialysis sampling for studying protein binding of drug. *Talanta* **2001**, *53*, 835-841.

(46) Okahata, Y.; Niikura, K.; Sugiura, Y.; Sawada, M.; Morii, T. Kinetic studies of sequence-specific binding of GCN4-bZIP peptides to DNA strands immobilized on a 27-MHz quartz-crystal microbalance. *Biochemistry* **1998**, *37*, 5666−5672.

JF052489R